IEEE Access
Multidisciplinary ⋮ Rapid Review ⋮ Open Access Journal

Received June 16, 2021, accepted June 21, 2021, date of publication June 25, 2021, date of current version July 5, 2021.

Digital Object Identifier 10.1109/ACCESS.2021.3092605

Diagnosis of Inter-Turn Faults Based on Fault Harmonic Component Tracking in LSPMSMs Working Under Nonstationary Conditions

ZAFER DOGAN, (Member, IEEE), AND KUBRA TETIK
Department of Electrical and Electronics Engineering, Tokat Gaziosmanpasa University, 60150 Tokat, Turkey
Corresponding author: Zafer Dogan (zafer.dogan@gop.edu.tr)

This work did not involve human subjects or animals in its research.

ABSTRACT Inter-turn faults are one of the most important issues in line-start permanent magnet synchronous motors (LSPMSMs). To date, steady-state operating conditions of LSPMSMs have been analyzed in studies focusing on diagnosing this fault. However, no studies have been conducted for nonstationary operating conditions, such as variable speed or variable load conditions, which are common in the industry. This paper presents a novel approach for fault harmonic component (FHC) tracking based on transient-MCSA to diagnose inter-turn faults in an LSPMSM operating under nonstationary conditions. First, the inter-turn failure model of LSPMS was analyzed to show the fault effect on motor current, and the most dominant inter-turn FHC in the order and frequency domains were determined. Then, using Gabor-OT, inter-turn FHC signals were extracted from motor current signals in the frequency domain and reconstructed in the time domain. Intrinsic mode functions (IMFs) were calculated by decomposing the reconstructed FHC signals (RFHCSs) via ensemble empirical mode decomposition. Using the energies of RFHCSs, calculated based on Gabor coefficients, and the Kullback–Leibler divergences of the selected IMFs, diagnosis of the inter-turn faults and detection of the severity of the faults was performed. The results are in agreement with the results in the literature, thus showing that the proposed method is a successful and useful means for detecting inter-turn faults in LSPMSMs.

INDEX TERMS Ensemble empirical mode decomposition, fault detection, gabor-order tracking analysis, line-start permanent magnet synchronous motors.

I. INTRODUCTION

A line-start permanent magnet synchronous motor (LSPMSM) is a hybrid motor with the best features of permanent magnet synchronous motors (PMSMs) and induction motors (IMs). Due to its advantages, such as line start without the need for a power electronic converter like an IM and high operational efficiency, LSPMSMs are increasingly replacing IMs in industrial areas [1].

One of the most important faults of LSPMSMs is stator winding faults, which account for approximately 36% of all motor faults [2], [3]. Various techniques based on parameters such as vibration [4], output torque [5], and current [1] have been used for the diagnosis of this fault; motor current signature analysis (MCSA) is the most widely used method [2], [6].

The associate editor coordinating the review of this manuscript and approving it for publication was Shihong Ding.

When the research into detecting LSPMSM winding faults is examined, there are model-based approaches [7]–[9], signal analysis methods [10], Artificial Neural Networks (ANNs), and Deep Learning [1], [11], [12]. In these studies, model-based approaches have been used most frequently. In previous studies on the diagnosis of LSPMSM stator winding faults [1], [7]–[12], the steady-state operating condition of the motor was considered, however, no research has been performed for nonstationary conditions. LSPMSMs, like many other motors in today's industrial environments, drive mechanical systems under variable speeds (ramp) and variable loads. Therefore, as the first research in this area, this paper has focused on the diagnosis of inter-turn failures of an LSPMSM operating under nonstationary conditions.

Due to the dynamic operating state caused by the hybrid rotor structure comprising the cage and magnets, the stator winding faults of LSPMSM are very difficult to detect.

In an LSPMSM with a winding fault, the asymmetries are formed in rotor currents in the start-up, whereas a magnetic flux is formed against the natural flux of permanent magnets in the rotor in the steady-state; these situations produce fault harmonic components (FHCs) in the motor current. These FHCs can be detected with the conventional MCSA in steady-state operating conditions of the motor [8], [11]. Because of the varying speed in an LSPMSM operating in nonstationary conditions, since both the frequency and amplitude of the current signal change over time, the detection of FHCs cannot be made using the conventional MCSA. Instead, the transient MCSA, as an extension of MCSA to transient conditions [13], should be used to analyze transient current signals in these conditions. The short-time Fourier transform (STFT) [14], Hilbert-Huang transform (HHT) [15], wavelet transform (WT) [6], Wigner-Ville distribution (WVD) [16], and Gabor transform [17] are methods to analyse the nonstationary signals. In these methods, a current signal in the time-domain (1D) is converted into a spectrogram in the t-f plane by special transform techniques [18]. However, there are some difficulties in spectrogram-based analyses of the signals of a motor operating under dynamic conditions. If the spectrograms of these signals are obtained by calculating the whole spectrum band through quadratic t-f transforms, then cross-term artifact problems may occur, which causes the loss of fault information due to the inability to move actual FHCs to the spectrogram produced [19]. These problems create significant difficulties in the detection and diagnosis of faults [18]. For the fault detection in a transient motor current signal, these problems can be solved by analyzing only the fault-related harmonic component of the signal, instead of analyzing a whole spectrum band [13], [20]–[22]. In recent studies, based on FHC tracking (FHCT) for fault diagnosis of other rotating electric machines operating under nonstationary conditions, model-based methods [23], Vold-Kalman filtering order tracking (VKF-OT) [16], frequency-tracking algorithm [24], etc. have been used.

This paper presents a novel FHCT method based on analysis of the motor current signals through Gabor order tracking (Gabor-OT) and Ensemble Empirical Mode Decomposition (EEMD) to diagnose inter-turn faults in an LSPMSM operating under nonstationary conditions. In this FHCT method based on transient MCSA, the waveform in the time domain of the FHC of current signal is reconstructed, and the reconstructed FHC signal (RFHCS) is obtained. Order tracking (OT) is an effective method to the FHCT in dynamic signals of rotary machines [25]. As described in [25] OT defines the order spectrum as the normalization of the rotational speed instead of a certain frequency. FFT-based OT [26], Computed OT [27] and Time-Variant DFT-based OT [25], which are classic OT methods, are non-reconstruction-based methods [28]. Therefore, they offer limited possibilities to the FHCT of a signal. VKF-OT [16], [28], and Gabor-O [29], which are modern OT techniques, are reconstruction-based methods. These methods are capable of reconstructing harmonic orders in their time history and extracting a specified frequency/order component. As time history allows instantaneous determination of values such as frequency and amplitude at any time, any FHC of a signal can be easily traced using these methods [14]. Although Gabor-OT and VKF-OT are the most accurate techniques for nonstationary signal analysis, their most important drawbacks are that they require excessive calculations. In [30], where these two methods were compared, it was stated that both methods are similar in terms of analysis results. However, it is worth mentioning that as it is clear in source [17], the Gabor-OT scheme is superior for reconstruction as it produces higher-resolution RFHCSs and gives smoother results than VKF-OT. In addition, the Gabor-OT can accurately decompose the separation of close and cross-order ratios and extract multiple-order ratios at the same time [27]. Gabor-OT is one of the most convenient tools for tracking the harmonics of nonstationary signals due to these advantages [18]. Therefore, the Gabor-OT was used to calculate the RFHCSs in this paper.

The RFHCS obtained via Gabor-OT for the FHCT of LSPMSM is also a nonstationary signal [31]. To detect the severity of the fault, the nonstationary signal can be analyzed by decomposing it into a more stationary waveform using various adaptive decomposing methods [32]. For a t-f signal analysis that addresses the true physical behavior of a system, empirical mode decomposition (EMD), an adaptive signal processing approach, is one of the most appropriate methods [15]. This technique decomposes a nonstationary signal into a set called intrinsic mode functions (IMFs), each of which is part of the original signal in a single-component narrow frequency band, through numerical approaches. However, due to the mode-mixing problem in EMD, ensemble EMD (EEMD) has been widely used in recent years to decompose the fault signals of rotary machines [32]. EEMD allows retrieving information on the characteristics of the signal by decomposing the signal more precisely and efficiently compared to the original EMD. Therefore, in this study, RFHCSs are analyzed through EEMD to determine the severity of the fault.

The application stages of the proposed fault diagnosis method are as follows. The most dominant frequency/order FHC was determined by analyzing the inter-turn fault model of a three-phase LSPMS to demonstrate the fault effect on motor stator current. Using the experimental setup established for fault detection, stator current signals in the healthy and faulty conditions of LSPMSM were monitored. Thereafter, the FHC was extracted from the motor current via Gabor-OT, and the RFHCS waveform was reconstructed in the time domain. The IMFs of RFHCSs were calculated using EEMD. Finally, using the energies of RFHCSs calculated based on Gabor coefficients, and the KLD of the selected IMFs, diagnosis of the inter-turn faults and detection of the severity of the faults was performed.

The novelty and contributions of this paper can be summarized as follows. 1. As mentioned above, there are currently no studies on the detection of stator winding faults of an LSPMSM operating in nonstationary conditions; this paper

is the first study in the literature. 2. The proposed diagnostic method is a novel approach for fault harmonic component tracking based on transient-MCSA. 3. To date, the Gabor-OT technique has not been used in the diagnosis of faults of this motor. 4. Because the proposed method is based on FHCT analysis, the change in electromagnetic noise caused by the operating environments of the motor does not affect the accuracy of the diagnosis. 5. OT analysis methods are mainly used for the diagnosis of mechanical malfunctions based on dynamic vibration signal analysis. However, in this study, Gabor-OT was proposed for electrical fault diagnosis based on the current signal. 6. The proposed method can continuously detect winding faults, unlike the conventional MCSA. Due to this feature, it can also be used for the diagnosis of incipient faults in motors such as winding faults, rotor broken bar faults, etc. In addition, the results obtained in this study were compared with the studies in the literature and presented in Section V.

The following sections of this article are organized as follows. The stator winding failure model of LSPMSM is presented in Section 2. The fault diagnosis approach is described in Section 3, experimental studies are explained in Section 4, results and discussions are presented in Section 5, and Section 6 explains the conclusions of the study.

II. MODEL OF THE LSPMSM CONSIDERING WINDING INTER-TURN FAULTS

In this section, the model of the inter-turn fault of LSPMSM is presented to determine the fault effect on the motor current. The behavior of rotary electric machines and the effects of fault conditions are analyzed using appropriate models [16]. In three-phase AC rotary electric machines, the *abc* stationary reference frame model is the most ideal model for stator winding failure [8]. The transient-state equations of a three-phase LSPMSM in the *abc* reference frame were given in [8] and [7]. By creating inter-turn faults to phase a of LSPMSM, these mathematical equations can be expressed as in [8] and [7]:

$$\begin{aligned}\left[V_{s,abcf}\right] &= \left[R_{sf}\right].\left[i_{s,abcf}\right] + \frac{d}{d_t}\left[\lambda_{s,abcf}\right] + \left[e_{abcf}\right],\\ \left[V_{r,abc}\right] &= \left[R_r\right].\left[i_{r,abc}\right] + \frac{d}{d_t}\left[\lambda_{r,abc}\right] = 0.\end{aligned} \tag{1}$$

It can be expressed as matrices in the above voltage equations:

$$\begin{aligned}\left[V_{s,abcf}\right] &= \left[\, v_a \;\; v_b \;\; v_c \;\; 0 \,\right]^T,\\ \left[i_{s,abcf}\right] &= \left[\, i_a \;\; i_b \;\; i_c \;\; i_f \,\right]^T, \quad \left[i_{r,abc}\right] = \left[\, i_a \;\; i_b \;\; i_c \,\right]^T,\\ \left[R_{sf}\right] &= \begin{bmatrix} r_s & 0 & 0 & -\mu.r_s \\ 0 & r_s & 0 & 0 \\ 0 & 0 & r_s & 0 \\ \mu.r_s & 0 & 0 & -(\mu.r_s + R_f) \end{bmatrix},\\ \left[R_r\right] &= \begin{bmatrix} r_r & 0 & 0 \\ 0 & r_r & 0 \\ 0 & 0 & r_r \end{bmatrix},\end{aligned}$$

$$\left[e_{abcf}\right] = \lambda_{pm}\omega_e.\left[\sin(\theta_r)\sin\left(\theta_r - \frac{2\pi}{3}\right) \times \sin\left(\theta_r + \frac{2\pi}{3}\right)\mu.\sin(\theta_r)\right].^T \tag{2}$$

Neglecting the leakage fluxes, the linkage flux of the stator and rotor can be expressed as a function of the rotor and stator currents as follows:

$$\begin{aligned}\left[\lambda_{s,abcf}\right] &= \left[L_{ss,abcf}\right].\left[i_{s,abcf}\right] + \left[L_{sr,abcf}\right].\left[i'_{r,abc}\right],\\ \left[\lambda_{r,abc}\right] &= \left[L_{rs,abcf}\right].\left[i_{s,abcf}\right] + \left[L_{rr,abc}\right].\left[i_{r,abc}\right].\end{aligned} \tag{3}$$

Inductance matrices in (3) can be expressed as follows:

$$\begin{aligned}&\left[L_{ss,abcf}\right]\\ &= \begin{bmatrix} L_{sa} & M_{sasb} & M_{sasc} & -(L_{sa_f} + M_{sa_hsa_f}) \\ M_{sbsa} & L_{sb} & M_{sbsc} & -M_{sbsa_f} \\ M_{scsa} & M_{scsb} & L_{sc} & -M_{scsa_f} \\ (L_{sa_f} + M_{sa_hsa_f}) & M_{sa_fsb} & M_{sa_fsc} & -L_{sa_f} \end{bmatrix}\\ &\left[L_{rr,abc}\right]\\ &= \begin{bmatrix} L_{ra} & M_{rarb} & M_{rarc} \\ M_{rbra} & L_{bs} & M_{rbrc} \\ M_{rcra} & M_{rcrb} & L_{cs} \end{bmatrix},\\ &\left[L_{rs,abc}\right]\\ &= \begin{bmatrix} M_{rasa} & M_{rasb} & M_{rasc} & -M_{rasa_f} \\ M_{rbsa} & M_{rbsb} & M_{rbsc} & -M_{rbsa_f} \\ M_{rcsa} & M_{rcsb} & M_{rcsc} & -M_{rcsa_f} \end{bmatrix},\\ &\left[L_{sr,abc}\right]\\ &= \begin{bmatrix} M_{sara} & M_{sarb} & M_{sarc} \\ M_{sbra} & M_{sbrb} & M_{sbrc} \\ M_{scra} & M_{scrb} & M_{scrc} \\ M_{sa_fra} & M_{sa_frb} & M_{sa_frc} \end{bmatrix},\end{aligned} \tag{4}$$

where the self and mutual inductances between short-circuited and healthy turn parts in phase a are $L_{sa_f} = 3\mu^2.L_{sa}$ and $M_{sa_hsa_f} = (\mu - 3\mu^2)L_{sa}$, respectively. In these equations, R_f is shorting resistor, connected in parallel to the phase a stator winding to create a fault; r_s and r_r are healthy state stator and rotor phase resistors, respectively; $\left[L_{ss,abcf}\right]$ and $\left[L_{rr,abc}\right]$ are inductance matrices for stator and rotor circuits, respectively; and $\left[L_{sr,abc}\right]$ and $\left[L_{rs,abc}\right]$ are the mutual inductance matrices between the stator and rotor. λ_m is the magnetic flux generated by permanent magnets and θ_r is the position angle of rotor. With the total number of turns, N, and short-circuit number, n, the ratio of short-circuited windings is $\mu = n/N$ in any phase. i_f is the fault current flowing through short-circuited turns n. The effect of healthy phases on the faulty phase is very small [33]; thus,

$$i_f \cong i_a\frac{(\mu + \mu.r_s)}{(\mu.r_s + R_f)} + \lambda_{pm}.\omega_e.\frac{\mu}{(\mu.r_s + R_f)}.\sin(\theta_r) \tag{5}$$

is obtained by arranging the fourth line of equation (1). In equation (5), the effect of permanent magnets on the faulty phase current is more predominant because the last term is more important [8], due to the induction effect of magnets on the rotor. In the case of synchronous operation of LSPMSM,

this effect induces the third harmonic, which is the characteristic inter-turn FHC of the fault current i_f [34], [35]. The third harmonic is the most dominant frequency component of the stator current of LSPMSM with inter-turn fault. A frequency spectrum of the stator current of a three-phase LSPMSM with inter-turn fault in phase *a,* operating under steady-state conditions, is shown in Figure 1.

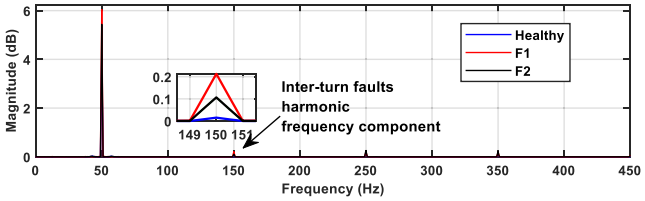

FIGURE 1. Frequency spectrum of the stator current of a LSPMSM with inter-turn fault operating under steady-state condition.

In the spectrum in Figure 1, the effects of inter-turn faults are clearly seen at FHC, which is the third harmonic component (150 Hz). As the severity of fault increases, the amplitude of the FHC increases, too. Therefore, inter-turn faults can be diagnosed by analyzing these FHC in the stator current frequency/order spectra.

III. FAULT DIAGNOSIS APPROACH

This section describes the procedure for performing the proposed FHCT analysis for the diagnosis of inter-turn faults of LSMSM operating under nonstationary conditions. The order spectrum of the stator current of a three-phase LSPMSM with the inter-turn fault in phase *a* operating under steady-state condition is shown in Figure 2.

The equivalent in the order domain of a certain x frequency component f_x in the frequency domain is calculated as:

$$l_x = \frac{(f_x.60)}{n_r} \tag{6}$$

According to this equation, the *3f* frequency component, which is the FHC of inter-turn fault in the frequency domain, corresponds to the 6th order in the order domain, see Figure 2. According to Figure 2, the amplitude of the 6th order changes in direct proportion to the change in the severity of the fault. In LSPMSMs operating under nonstationary conditions, making a reliable fault diagnosis decision, and correctly determining the severity of fault, depends on the correct reconstruction of the inter-turn FHC signal in the time domain. Gabor-OT is a useful tool for this purpose. The proposed FHCT approach is based on the analysis by extracting the 6th order component, the most dominant inter-turn FHC, from the motor current using Gabor-OT.

Figure 3 summarises the implementation of the proposed FHCT for the diagnosis of inter-turn faults of LSMSM operating under nonstationary conditions. Application stages of the proposed FHCT are described in the following sections.

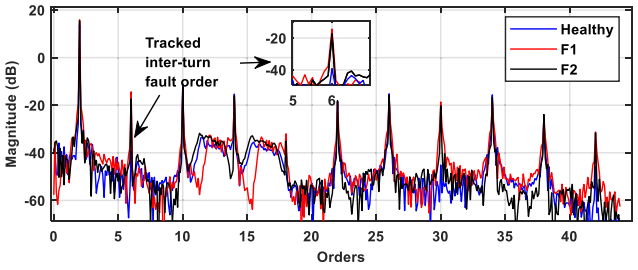

FIGURE 2. Order spectrum of the stator current of a LSPMSM with inter-turn fault operating under steady-state condition.

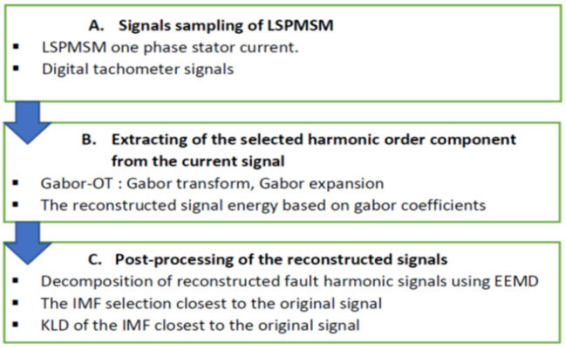

FIGURE 3. Application scheme of the proposed FHCT.

A. SIGNAL SAMPLING OF LSPMSM

At this stage, one phase stator current signal $i(t)$ and the digital speed data $p(t)$ of a three-phase LSPMSM are sampled simultaneously at sampling frequency f_s during the sampling period t_s. The sampled current and digital speed signals obtained from the Test 1 experiment of an LSPMSM with inter-turn fault operating under nonstationary conditions, which is driven by a variable speed driver, are shown in Figure 4 (a) and (b). The Test 1 experiment details are given in detail in Section IV of this study.

B. EXTRACTING THE SELECTED HARMONIC ORDER COMPONENT FROM THE CURRENT SIGNAL

Gabor-OT is based on the principle that each signal can be expressed as a weighted sum of time and frequency function [4], [30]. This method is based on STFT with Gabor expansion. Gabor-OT, as one of the forward and inverse time-frequency transformations, makes it possible to get an idea of the time-varying behavior of the analyzed signal, and it enables the reconstruction of the waveform of a specified order component through Gabor expansion. The mathematical expressions of the Gabor transformation pair, comprising Gabor transform and Gabor expansion, have been established in detail in [30] and [36]. The Gabor expansion of one phase current signal of an LSPMSM with the inter-turn fault in a phase stator winding is defined as follows:

$$i\,(t) = \sum_{m=-\infty}^{\infty} \sum_{n=-\infty}^{\infty} I_{m,n} h_{m,n}\,(t), \tag{7}$$

where $I_{m,n}$ are the Gabor coefficients. Gabor elementary function, $h_{m,n}\,(t)$, is $h_{m,n}\,(t) = h(t - n.T)e^{j2\pi.\Omega.t}$, $m,\ n \in \mathbb{Z}$,

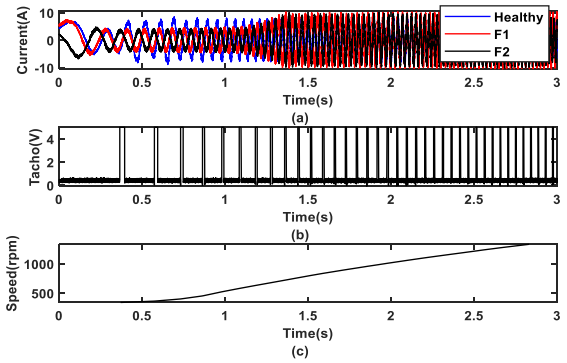

FIGURE 4. Sampled signals of a LSPMSM with inter-turn fault operating under nonstationary conditions: (a) Healthy and fault conditions phase currents for the motor, (b) digital speed signal, (c) speed graph as calculated using Gabor-OT.

where the function $h(t)$ is called the synthesis window, and T and Ω are lattice parameters. The Gabor transform of this signal is defined as follows:

$$i_{m,n} = \int_{-\infty}^{\infty} i\,(t)\gamma^{*}_{m,n}\,(t)\,e^{-jn\Omega t}, \tag{8}$$

where $m, n = 0, \pm1, \pm2, \ldots, \gamma_{m,n}(t) = \gamma(t - nT)e^{jm\Omega t}$ is the time and frequency shifted version of $\gamma(t)$, called analysis window, which is the Gabor transformation pair function of $h(t)$, and $*$ represents a complex conjugation. One of the most interesting applications of the Gabor expansion is filtering at changing times and is used to perform a recalculation of waveforms of certain order components [37].

The Gabor-OT method is a multi-stage process, which is used to extract a special-order component for the fault diagnosis of rotating machines. First, the time and frequency steps of signals necessary for the discretization process of the sampled signals of LSPMSM are defined as:

$$\Delta t = \frac{t_s}{N} = \frac{1}{f_s}, \quad \Delta f = \frac{f_s}{N} = \frac{1}{t_s}, \tag{9}$$

where N is the total number of samples. Second, the selection of process parameters and the calculation of Gabor coefficients are performed. The most fundamental problem in Gabor OT-based signal analysis of rotating electric machines operating in nonstationary conditions is the selection of synthesis window, analysis window, and lattice parameters [18]. In Gabor expansion, significant concentration and resolution issues occur if the appropriate synthesis window is not selected [36]. In the present study, the Gaussian window [18] with the Heisenberg box, which can provide the highest energy concentration in the smallest area in the t-f plane, was preferred as the synthesis window. Numerical instabilities arise in the calculation of Gabor coefficients performed using a critically sampled lattice. To solve this problem, maximum oversampling on the t-f plane has to be ensured when the coefficients $I_{m,n}$ in (8) are calculated. In the selection of T and Ω parameters, if the $T.\Omega \rightarrow 0$ condition can be met, the window can be shifted with maximum overlap. In this case, the synthesis window $h(t)$ is the same as analysis window $\gamma(t)$ [30]. The Gabor elementary function given in (7) is regulated as follows, taking the lattice parameters as $T = \Delta t$ and $\Omega = \Delta f$ for maximum oversampling,

$$h_{m,n}\,(t) = h(t - n.\Delta t)e^{j2\pi\,\Delta f\,.m.t}, \quad m, n\epsilon\mathbb{Z}. \tag{10}$$

Using the selection considering the maximum oversampling, the Gabor transform in (8) is regulated as follows [18], [36]:

$$i\,[m, n] = \sum_{k=0}^{N-1} i\,[k]h\,[k-n]\,e^{-j\frac{2\pi mk}{N}}, \quad 0 \leq m, n < N, \tag{11}$$

and Gabor coefficients $i\,[m, n]$ are calculated as an NxN matrix, where $i[k]$ and $h[k]$ are discrete arrays with N elements obtained via the sampling of the motor current $i(t)$ and Gabor elementary function $h_{m,n}\,(t)$ with the constants $t = k.\Delta t$ and $0 \leq k \leq N - 1$. Third, a Gabor spectrogram is created by mapping the Gabor coefficient array to the 2D image. The density of each lattice in the image represents the amplitude of $c_{m,n}$ at a specific time m and a specific frequency n. To obtain a high-resolution image, N must be selected as a large value. However, in this case, the transform calculation in (11) takes a long time. Gabor spectrogram of the stator current of an LSPMSM with inter-turn fault operating under nonstationary conditions, seen in Figure 4(a), is given in Figure 5.

In this spectrogram, created using all Gabor coefficients obtained from the Gabor transform in equation (11), all of the order components of the stator current of an LSPMSM in F1 inter-turn fault state, operating under nonstationary conditions, can be clearly seen. This figure also shows the time-varying frequency of any order component. The 2^{nd} order is the supply order corresponding to the supply frequency. The 6^{th} order shows the traced inter-turn FHC. In addition, because of the visual advantage of the Gabor spectrogram, 10^{th}, 14^{th}, 22^{nd}, 26^{th}, 30^{th}, 34^{th}, and 38^{th} orders can be clearly seen. As mentioned above, a clear image is obtained in Figure 5 due to the selected Gabor parameters. The selection of Gabor parameters and the F1 inter-turn fault state of LSPMSM used in this study is detailed in Section IV. Fourth, the rotational speed $w(t)$ versus tachometer pulse position seen in Figure 4(c) is calculated as per the expression $w(t) = d\theta/dt$; accordingly, the rotative speed is calculated as $n_r{=}2\pi/(\omega\,(t)\,60)$. Fifth, a masking process is performed on the Gabor coefficient sequence obtained through equation (11), using the rotary speed n_r and a specific x order l_x. The position index of the specified order lx in the Gabor time-frequency lattices is defined as:

$$index\,(l) = lap\left(\frac{n_r}{60}\frac{N}{fs}l\right), \quad l\epsilon\mathbb{N}^{+}, \tag{12}$$

where '*lap*' is the number of completed rotations. In the masking process, a masking window with a specific bandwidth is used, whose center frequency is determined by n_r and l_x. In the mask window, a $w\,[m, n]$ mask matrix with a

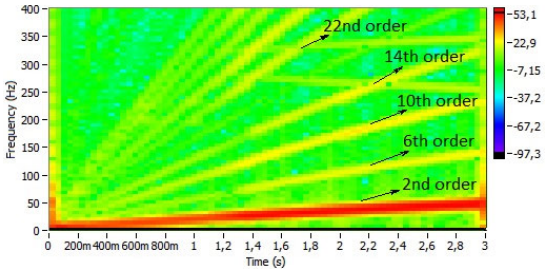

FIGURE 5. Gabor spectrogram of motor current signal for F1 fault.

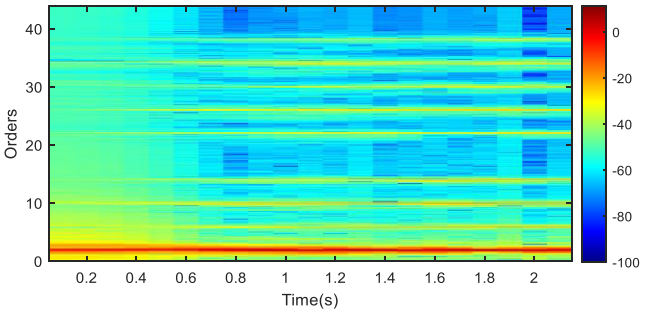

FIGURE 6. Gabor Spectrogram of RFHCS of the traced inter-turn FHC for F1 fault.

value limited to 0 or 1 is generated with the same dimension as that of the Gabor coefficient matrix $i[m, n]$. The Gabor coefficient matrix, $i[m, n]$, is only multiplied by a mask window for the purpose of keeping the *index(l)* coefficients calculated using equation (12). It acts as a mask by preserving $i_{m,n}$ when $w_{m,n} = 1$ and removing $i_{m,n}$ when $w_{m,n} = 0$. The coefficients corresponding to $w_{m,n} = 1$, make up the mask region. As a result, equation (13) shows the modified Gabor coefficient matrix [37],

$$\hat{i}[m, n] = \begin{cases} i_{m,n} & w_{m,n} = 1 \\ 0 & w_{m,n} = 0 \end{cases} \tag{13}$$

Sixth, a '*Waveform reconstruction*' process is performed through Gabor expansion, given equation (7). For reconstruction, the synthetic window function that is regulated for maximum oversampling, *h[k],* given in (10), and the modified Gabor coefficients, $\hat{i}[m, n]$, are used. The masking process described above means that the reconstruction process will only allow the re-construction in the time domain of the desired FHC of the motor current signal. Using a lattice with maximum oversampling in equation (7), the time history of a specified order l is reconstructed as:

$$i_{f,x}[k] = \sum_{m=0}^{N-1} \sum_{n=0}^{N-1} \hat{i}[m, n] h[k-n] e^{j\frac{2\pi mk}{N}}, \quad 0 \le k < N \tag{14}$$

where $i_{f,x}[k]$ is RFHCS, as a discrete array [18], [36]. Finally, the time form of a certain order l_x can be expressed as:

$$i_{f,x}(t) = \sum_{m\in\mathbb{Z}} \sum_{n\in\mathbb{Z}} \hat{i}_{m,n} h(t - n.\Delta t) e^{j2\pi \Delta f.m.t} \tag{15}$$

where $i_{f,x}(t)$ is RFHCS of the traced inter-turn FHC in the time domain [36]. This signal is also the $i_{RFHCS}(t)$ signal. The energy of any harmonic order component of a signal in t-f plane transformations generated by the modified Gabor coefficients,

$$Energy\left(i_{f,x}(t)\right) = \sum_{m\in\mathbb{Z}} \sum_{n\in\mathbb{Z}} \left|\hat{i}_{m,n}\right|^2, \tag{16}$$

is an important signal feature [4], [17], [18], [30]. To better present the importance of this feature in the proposed FHCT application, the Gabor spectrogram of the 6th order component seen in Figure 5 is given in Figure 6.

In this spectrogram, created using the modified Gabor coefficient, the 6th order component is seen in time-order graphs. It also shows maximum energy calculated according to equation (16) of the order for each *ti*. Using this spectrogram, the energy of the order at any time can be determined. In this figure, the 6th order maximum energy level is -10 dB. This parameter is an important indicator that can provide information about the fault condition of the motor. Therefore, in this study, the energy of RFHCS (the 6th order), which is the most dominant inter-turn FHC in a phase current of a winding fault LSPMSM, is used as a reliable fault indicator.

C. SENSITIVITY ANALYSIS

The RFHCSs calculated through Gabor-OT in (15), of an LSPMSM with inter-turn fault working under nonstationary conditions, are dynamic signals. The most reliable approach in analyzing such signals is to obtain the properties of the stable forms of the signal [32]. EMD is one of the most effective methods used to decompose nonstationary signals [15]. This technique, as in many other fields [38], is widely used in the fault diagnosis of electrical machinery [32], [39], [40]. EMD extracts a series of IMFs with local characteristics of a nonstationary signal, which is analyzed by gradually shifting EMD, and a current signal can be decomposed as $i_{f,x}(t)$ as follows:

$$i_{f,x}(t) = \sum_{i=1}^{j} IMF_i(t) + r(t), \tag{17}$$

where $r(t)$ is j^{th} IMF and a non-zero mean residue and $IMF_i(t)$ is i^{th} IMF. This decomposition algorithm can be summarised as follows:

- Determination of all local extrema of $i_{f,x}(t)$ current,
- Obtaining upper (e_{max})/lower (e_{min}) envelopes through interpolation,
- Calculation of the mean envelope by using e_{max} and e_{min} envelopes,
- Calculation of candidate IMF $g_k(k)$ by subtracting the mean envelope from $i_{f,x}(t)$,
- Iteration process on the $r(t)$ residue.

This algorithm is re-determined through an elimination process until $g_k(k)$ is recognized as an IMF. However, the drawbacks of EMD include: the occurrence of the mixing mode phenomenon, noise sensitivity, and mathematical modelling difficulty. To deal with these drawbacks, ensemble EMD (EEMD), a noise-assisted data analysis method, has been

proposed [32], [40]. In this method, the decomposition process is performed by adding white noise to the original signal series so that signals of different scales can be automatically separated according to their respective reference scales. The EEMD algorithm of a current signal can be summarised as follows:

- Create the signal $i^c_{f,x}(t)$ by adding white noise $\beta w^c(t)$ to $i_{f,x}(t)$,
- Decompose the signal $i^c_{f,x}(t)$ via EMD to obtain IMF components,
- Repeat the first and second steps by adding a new white noise,
- Obtain the result by calculating the mean of IMFs obtained in each iteration.

The Pearson correlation approach, which establishes a relationship between the two signals, based on the values of the coefficient of correlation, r, ranging from -1 to 1, was used in the selection of the obtained IMFs. r is expressed as:

$$r = \frac{\sum x_i y_i - \frac{\sum x_i \sum y_i}{n}}{\sqrt{\left(\sum x_i^2 - \frac{(\sum x_i)^2}{n}\right)}\sqrt{\left(\sum y_i^2 - \frac{(\sum y_i)^2}{n}\right)}} \tag{18}$$

D. FAULT DETECTION CRITERION

The Kullback-Leibler Divergence (KLD) is statistical information that is used as a measure of proximity between two distributions. It is used in many areas such as pattern recognition, fault detection, and anomaly diagnosis [41]. In previous signal processing studies where KLD has been compared with traditional statistical methods such as Hotelling T^2, SPE, and Q [42], [43], it has been revealed that KLD provides the most sensitive results for fault diagnosis. The dissimilarity between the probability density functions (PDFs) of the current signals of an LSPMSM at healthy condition and fault condition, $p_{h(w)}$ and $p_{f(w)}$, respectively, is defined as:

$$I\left(p_h \backslash\backslash p_f\right) = \int p_{h(w)} \log\left(\frac{p_{h(w)}}{p_{f(w)}}\right) dw. \tag{19}$$

Since the Kullback-Leibler distance is unidirectional according to the given two probability distributions, KLD is expressed as

$$I_{KDL} = I\left(p_h \backslash\backslash p_f\right) + I\left(p_f \backslash\backslash p_h\right). \tag{20}$$

I_{KDL} is not negative, but if the distribution of two probabilities is identical, then 0. So I_{KDL} takes the value 0 in absolute similarity and 1 in the case of absolute dissimilarity.

IV. EXPERIMENTAL SETUP FOR THE PROPOSED METHOD

For verification of the proposed fault diagnosis method, tests were performed using a commercial LSPMSM. The intern-turn winding fault was created by connecting a rheostat in parallel to a coil of phase a of the motor. In the healthy condition of the motor, the winding resistance of phase a was 2.2 ohms. In the motor for experimental studies, two different levels of fault states (F1 and F2) were formed. The winding resistances of phase a of the motor in the F1 and F2 failure states were 2.1072 and 2.1526 ohms, respectively. The LSPMSM was mounted on a test bench, which can reproduce different operating conditions. The test bench and its components are presented in the following section.

A. TEST BENCH AND THE SELECTION OF GABOR-OT PROCESS PARAMETERS

The connection diagram of the test bench and its components is shown in Figure 7. The parameters of the LSPMSM are given in the Appendix.

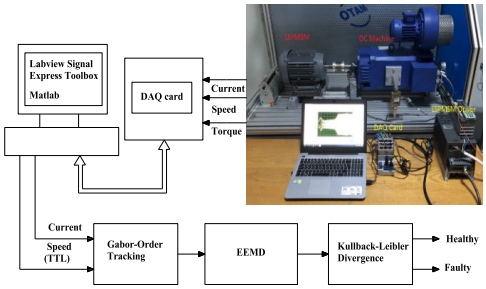

FIGURE 7. Connection diagram of the test bench and its components.

The motor was fed through a drive with scalar and direct torque control features. The digital velocity (TTL) data of the motor was measured using an inductive speed sensor. A DC machine, which was used as the mechanical load, was controlled by a DC machine driver. NI 9174 compact DAQ and NI 9227 were used as data acquisition and current modules, respectively. These modules have a hardware notch filter to eliminate electromagnetic waves and other noise. The data collection was conducted simultaneously from each channel with a sampling frequency of 25 kS/s. The current and digital velocity signals were collected under different load conditions (Load 1 (0%), Load 2 (50%), Load 3 (100%), and Load 4 (115%)) for healthy and faulty conditions of the motor. The signals received from sensors were transmitted via a DAQ card to the LabVIEW Signal Express Toolbox environment for real-time data collection and analysis and were saved to the computer in Excel format. The recorded data were visualized as graphs in the MATLAB environment.

As detailed in Section 3.1, the selection of parameters is important in Gabor-OT-based fault diagnostics. In this study, a Gaussian window with Heisenberg box was chosen as the synthesis window. Data acquisition parameters used for the tests were the sampling frequency (25 kHz), and the total sampling time ts ($ts = 3$ s for Test 1, $ts = 8$ s for Test 2). The lattice parameters for maximum oversampling were $T = \Delta t$ and $\Omega = \Delta f$.

B. EXPERIMENTAL TESTS

An LSPMSM with an inter-turn fault in phase a stator winding has been tested for three scenarios as follows:

a. *Test1(the ramp speed test)*: Acceleration in constant load conditions -no-load (0%), half-loaded (50%), full load (100%), and overload (115%)- with 3-s ramp from 0 to 1500 rpm.

b. *Test2(the ramp load test)*: In 1500 rpm constant speed, from no-load to full load, loading 8-s with stepped ramp.

c. *Test3(the test of incipient fault diagnosis)*: Suddenly the F1 fault-state at 3.65 s of the healthy motor operating in 1500 rpm and full load condition.

V. RESULTS AND DISCUSSION

A. THE GABOR-OT RESULTS

For the nonstationary operating conditions of the motor, the Gabor-OT results applied to the currents measured in Test 1 (Load 3) and Test 2 are given in Figure 8 and Figure 9, respectively.

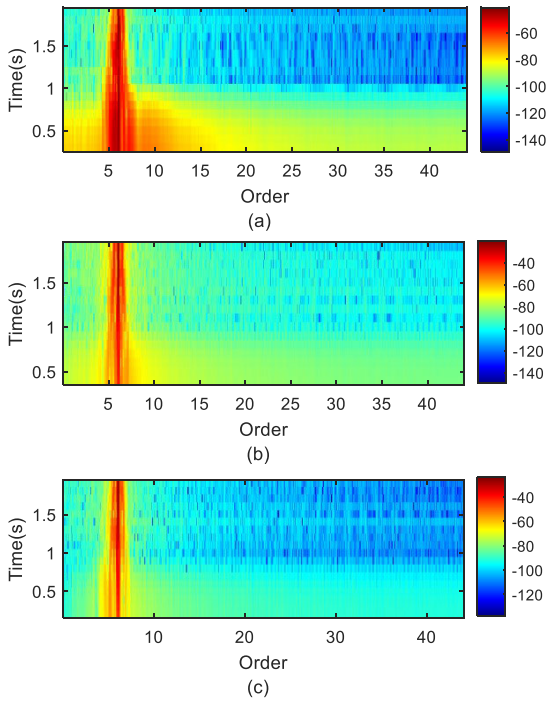

FIGURE 8. Gabor-OT results for test 1 (100% load): (a) Healthy Condition, (b) F1 fault condition, (c) F2 fault condition.

In these graphs, the spectrograms of LSPMSM as the order corresponding to the maximum energy calculated according to equation (16) for each time t_i of the RFHCS (the 6^{th} order component), which is the most dominant inter-turn FHC, is observed.

In the classical MCSA based t-f spectrograms, the inter-turn FHCs of a motor are constantly changing due to nonstationary conditions. Therefore, calculating these frequency components to diagnose the fault at each small interval of time is difficult. However, the inter-turn FHC is fixed in the 6^{th} order regardless of the dynamic state of the motor. Moreover, as can be seen from Figure 8 and Figure 9, the energy of the 6th order varies depending on the fault condition of the motor as a significant indicator of the fault.

The energies and KLDs of RFHCSs, which are inter-turn fault indicators for Gabor-OT results obtained from currents measured in Test 1 and Test 2, are given in Figure 10. In the

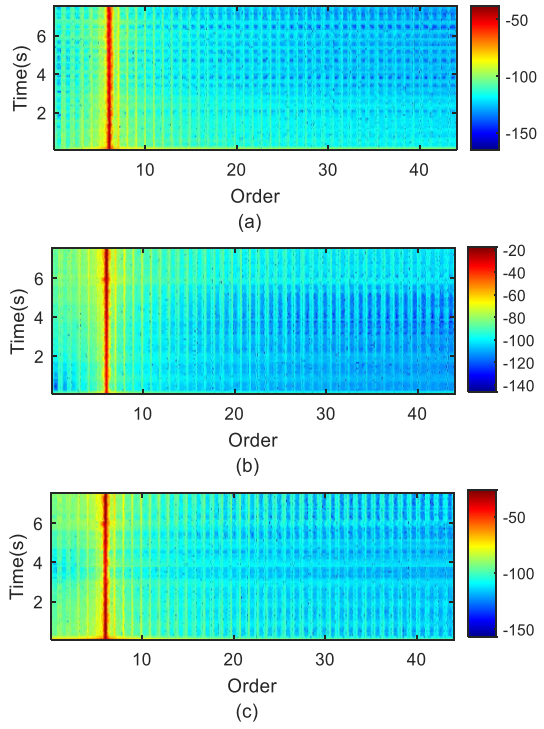

FIGURE 9. Gabor-OT results for test 2: (a) Healthy condition, (b) F1 fault condition, (c) F2 fault condition.

energies in Figure 10 (a), which shows the results of Test 1 for different load conditions, the average difference between healthy and F2 fault states is 13.375 dB, while this difference between F1 and F2 fault states is 1.9525 dB. Especially in the condition of 115% load, the energies of F1 and F2 fault states are very close to each other. Similar results are also seen in Figure 10 (b), which is presented as Test 2 results. In the KLDs of RFHCS seen in Figures 10 (c), the average difference between healthy and F2 fault states is 0.126552, and this difference in Figure 10 (d) is 0,180849. These results show that the changes in the KLDs and the changes in the energy plots are similar.

According to the results obtained in these graphs, although the healthy state of the motor can be easily distinguished from the fault states, the small difference between the fault level values of F1 and F2 states makes the determination of the severity of the fault difficult. These results showed that Gabor-OT is a powerful tool for diagnosing winding failure, but partly inadequate in determining the severity of the fault. Therefore, sensitivity analyses were performed to determine the severity of faults.

B. SENSITIVITY ANALYSIS RESULTS

In this section, the results of the proposed EEMD method for evaluating the severity of faults are presented. In Figure 11, the decomposed IMFs via EEMD of RFHCSs ($i_{RFHCS}(t)$) obtained from the currents measured for Test 1, are given. The first subplots of the graphs in Figure 11 show the RFHCSs. In these graphs, each IMF has a different frequency value. This result shows that EEMD decomposes high and

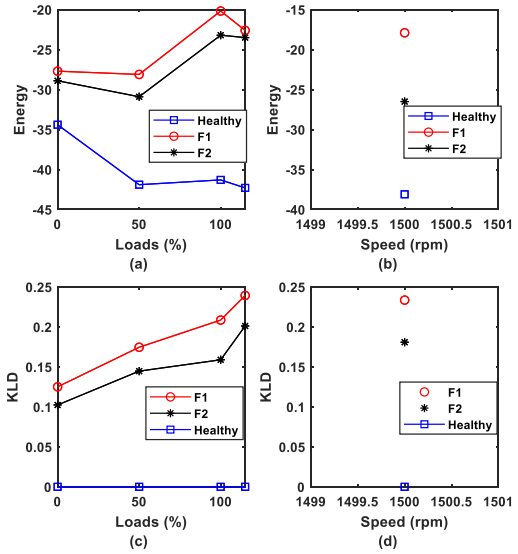

FIGURE 10. Inter-turn fault indicators for Gabor-OT results: (a) Energies in the RFHCSs for test 1. (b) Energies in the RFHCSs for test 2. (c) KLDs of RFHCSs for test 1. (d) KLDs of RFHCSs for test 2.

low-frequency components without mode-mixing problems. At the same time, nonstationary signal decomposition has also been tested for the adaptability of EEMD.

The RFHCSs obtained from the currents measured in Test 1 and Test 2 were decomposed by EEMD at 10 levels and 16 levels, respectively (including the residue signal). The IMFs closest to the original signals were selected to determine the severity of the fault in the motor. The closest IMFs to the original signals calculated using equation (17), of the IMFs produced by this decomposition, are given in Figure 12.

The values seen in Figure 12 (a), given for Test 1, are ordered according to Load 1 (0%), Load 2 (50%), Load 3 (100%) and Load 4 (115%) load conditions as follows: Healthy case IMF2, IMF1, IMF2 and IMF2; F1 failure state IMF2, IMF1, IMF2, and IMF2; F2 failure state IMF2, IMF1, IMF1 and IMF2. In Figure 12 (b) given for Test 2, these results are shown as IMF2, IMF1, and IMF1 for the healthy, F1 fault, and F2 fault states of the motor, respectively.

The KLD (I_{KDL}) results, calculated using equation (20) of healthy state PDF versus fault state PDF for each selected IMF for Test 1 and Test 2, are given in Figure 13. The KLD values vary in the range of 0 to 1. The absolute similarity is 0, and the absolute dissimilarity is 1 [43]. Considering this classification of information, while fault diagnosis has been performed using the values taken by the fault state KLD (according to the healthy state KLD values), the fault severity was determined using the differences between the F1 and F2 fault state KLDs.

As can be seen in Figure 13, for Test 1, as the KLD of selected IMFs, the average difference between the KLD values of F1 and F2 fault states in all load conditions of the motor is 0.2951. However, this value is 0.0351 in

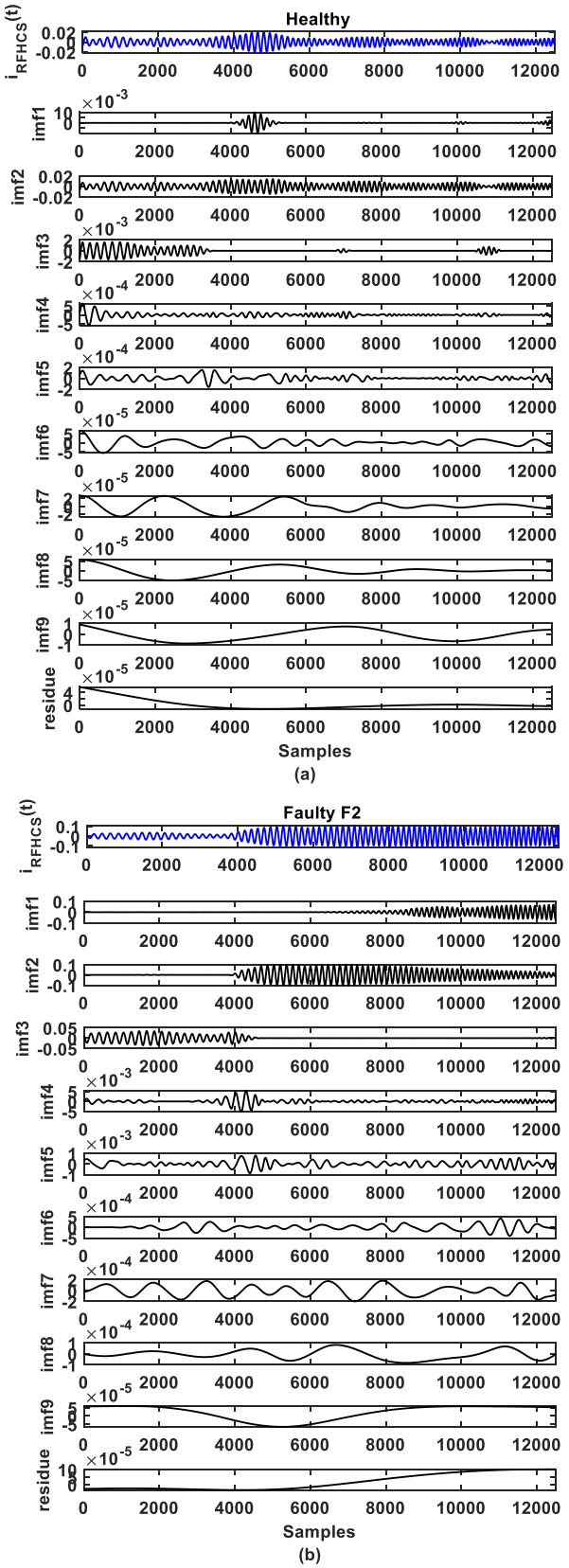

FIGURE 11. EEMD results of the RFHCSs for test 1 (100% load): (a) healthy state, (b) F2 fault state, and (c) F1 fault state.

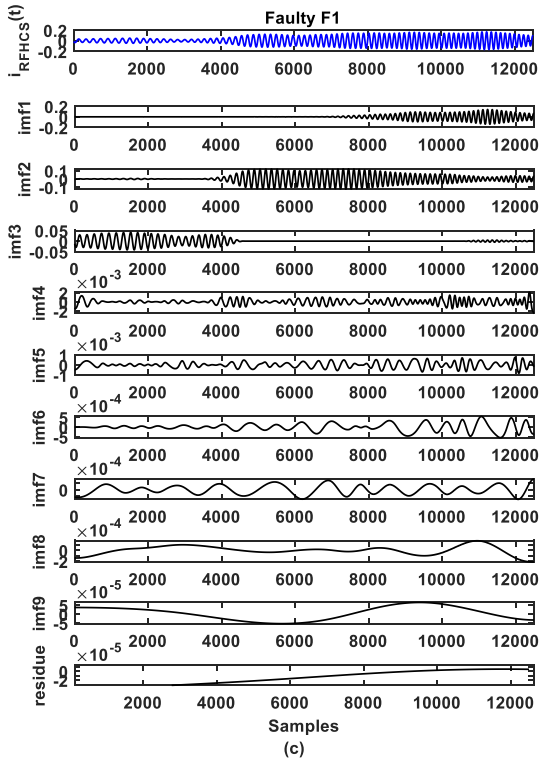

FIGURE 11. *(Continued.)* **EEMD results of the RFHCSs for test 1 (100% load): (a) healthy state, (b) F2 fault state, and (c) F1 fault state.**

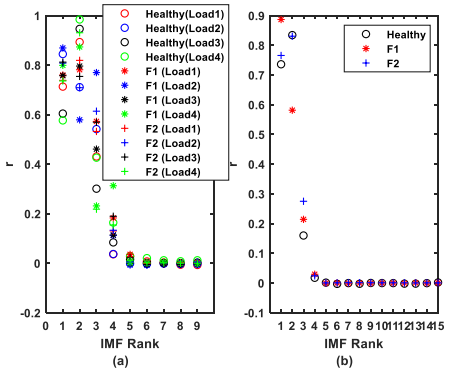

FIGURE 12. **The RFHCSs of motor states and correlations between their IMFs: (a) test 1 results, and (b) test 2 results.**

Figure 10 (c), for Test 1 as Gabor-OT results. Similarly, for Test 2, this average difference was 0.0527 in Figure 10 (d) and 0.3244 in Figure 13 (b). According to the results of the KLDs of selected IMFs obtained from the EEMD analyses of the RFHCSs, the severity of faults can be easily diagnosed for both Test 1 and Test 2.

As mentioned in Section 1, this is the first research paper regarding the detection of inter-turn faults of an LSPMSM operating in nonstationary conditions, such as ramp load and ramp speed. Therefore, in comparing the method proposed here with other methods in the literature, the studies made for the FHCT in the other motors operating in nonstationary conditions are considered. The obtained results are coherent with the results found in the literature [16], [23], [24], [34], [44].

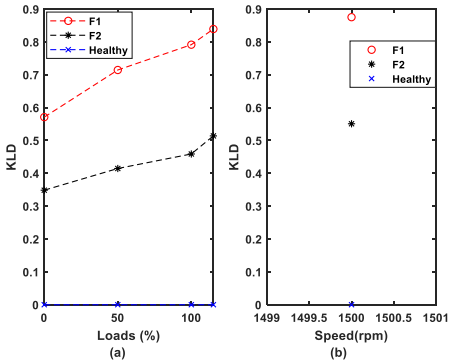

FIGURE 13. **Fault severity indicators according to selected IMFs obtained from the EEMD analyses of the RFHCSs: (a) KLDs for test 1, and (b) KLDs for test 2.**

In [16], where VKF-OT-based winding fault diagnosis was performed at a PMSM operating under dynamic conditions, the changes in third harmonics of the current signals for the healthy state, light fault state, and severe fault state are 0.004, 0.0125, and 0.0275 dB, respectively (under ramp conditions with a variable speed of 3500-5000 rpm). The change rates in these results are consistent with the values given in Figure 13. Moreover, for the diagnosis of a winding fault, based on motor currents, comparing the results of VKF-OT analysis obtained in [16] under 100-1500-rpm ramp conditions and the results obtained for Test 1 (0-1500 rpm ramp) in this study, the proposed Gabor-OT based fault diagnosis results are more precise and accurate. Furthermore, the 3rd harmonic presented in [44] as the most sensitive harmonic of stator currents for detecting inter-turn faults in PMSM, has been verified with the results obtained, to be a useful detection indicator for diagnosing LSMPM inter-turn faults. However, as special winding configurations affect other harmonics besides the third harmonic, the method proposed can be used to analyze the other current harmonic components too [34]. [24] proposed a frequency-tracking algorithm method for FHCT. While the average difference between healthy and fault states of the motor is 0.12166, in Figure 10 (b), which shows the inter-turn fault indicator for the Gabor-OT results in this paper, this value is 0.126552 in [24]. Compared with the results in Figure 10 (b), the fault indicators proposed in [24] are less effective for inter-turn diagnostics.

The model-based diagnostic approach that provides high sensitivity and accuracy in detecting incipient faults, such as winding faults, broken rotor bar faults, etc., is often used to diagnose faults in motors working under dynamic conditions [23], [43], [45]. To compare the fault diagnosis method proposed here with model-based methods, the incipient winding failure test (Test 3) was performed in the experimental studies. The measured currents for Test 3 and the Gabor-OT results obtained from these currents are given in Figure 14.

As can be seen from the Gabor spectrogram in Figure 14., the sudden failure situation (around t = 3.65s) caused an energy change in the 6th order, which is the inter-turn FHC, at the start of the failure. This result shows that this proposed

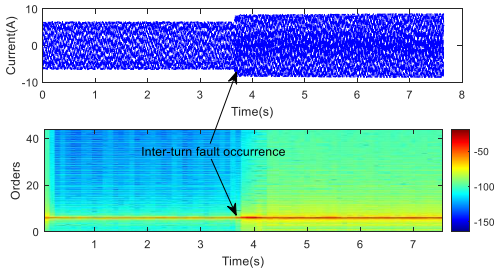

FIGURE 14. Gabor-OT results for test 3.

new diagnostic method can successfully diagnose incipient inter-turn faults. Compared with the changes of energy in the 6th order in Figure 14, the changes of *dq*-axis space vector in [23] are similar results for incipient inter-turn diagnostics. In addition, the results in Figure 14 are very close to those given in [45] for diagnosing an incipient winding failure of an induction motor.

According to all of the results, the success of the proposed fault diagnostic method depends on the correct selection of the Gabor-OT parameters necessary to obtain the matching window and oversampled lattice features. Otherwise, since the RFHCS cannot be correctly extracted from the motor current, the reliability of the diagnosis will decrease. This is the most important difficulty with the proposed method. In addition, this method also has other disadvantages. The excessive calculation problem expressed in VKF-OT-based diagnostic studies [16], [28] is also present in Gabor-OT. Gabor-OT needs motor digital speed information as a second signal, as well as motor current signals used for fault diagnosis, and as a result, the amount of data to be used for fault diagnosis increases. In such a case, problems arise such as large memory requirements for the creation of historical data records and data transmission disadvantages in online condition monitoring [13].

VI. CONCLUSION

In this paper, a novel FTCT method has been proposed, based on transient-MCSA, to diagnose inter-turn faults in an LSPMSM operating under nonstationary conditions, such as variable loads and speeds. Through a test bench established, the current and digital velocity signals of LSPMSM were collected. The FHC was extracted from the motor current via Gabor-OT, and the RFHCS waveform was reconstructed in the time domain. The obtained results have shown that the KLD values and energies of RFHCS were reliable fault indicators.

Comparing the Gabor-OT results and the results VKF-OT, which is shown as a competitor to Gabor-OT in the literature, it was seen that Gabor-OT was superior in the ramp speed condition of the motor. Furthermore, as the proposed method is based on FHCT analysis, the electromagnetic noise caused by the environments does not affect the accuracy of the diagnosis. The proposed method can continuously detect winding faults in both transient and steady-state, unlike conventional MCSA. Due to this feature, it can also be used for the diagnosis of incipient winding faults. However, despite these advantages, the difficulty of calculation is a major drawback of the proposed method.

As suggestions for future studies, multiple faults in motors that can occur in industrial areas might be diagnosed using the proposed method. The demagnetization faults might be detected in the LSMPSM with the proposed method. Since the proposed method is based on tracking harmonic components, this method can also be used in the analysis of harmonic components of voltage signals produced by generators.

APPENDIX

Line Start Permanent Magnet Synchronous Motor parameters: Rated characteristics: $P = 2.2$ kW, $f = 50$ Hz, V $(\Delta/Y) =$ 230/400 V, $I(\Delta/Y) = 7.1/4.4$ A, and $n = 1500$ rpm, Cos $\Phi =$ 0.85, Number of Poles $= 4$, % Efficiency $= 91.2$, Protection Class $=$ IP 54.

REFERENCES

[1] L. S. Maraaba, Z. M. Al-Hamouz, and M. A. Abido, "An accurate tool for detecting stator inter-turn fault in LSPMSM," *IEEE Access*, vol. 7, pp. 88622–88634, 2019, doi: 10.1109/ACCESS.2019.2923812.

[2] H. A. Toliyat, S. Nandi, S. Choi, and H. Meshgin-Kelk, *Electric Machines: Modeling, Condition Monitoring, and Fault Diagnosis*. New York, NY, USA: CRC Press, 2013.

[3] W. Liu, L. Liu, I.-Y. Chung, D. A. Cartes, and W. Zhang, "Modeling and detecting the stator winding fault of permanent magnet synchronous motors," *Simul. Model. Pract. Theory*, vol. 27, pp. 1–16, Sep. 2012, doi: 10.1016/j.simpat.2012.04.007.

[4] M.-C. Pan and C.-C. Chiu, "Investigation on improved Gabor order tracking technique and its applications," *J. Sound Vib.*, vol. 295, nos. 3–5, pp. 810–826, Aug. 2006, doi: 10.1016/j.jsv.2006.01.046.

[5] A. Siddique, G. S. Yadava, and B. Singh, "A review of stator fault monitoring techniques of induction motors," *IEEE Trans. Energy Convers.*, vol. 20, no. 1, pp. 106–114, Mar. 2005, doi: 10.1109/TEC.2004.837304.

[6] M. El Hachemi Benbouzid, "A review of induction motors signature analysis as a medium for faults detection," *IEEE Trans. Ind. Electron.*, vol. 47, no. 5, pp. 984–993, Oct. 2000, doi: 10.1109/41.873206.

[7] L. Maraaba, Z. Al-Hamouz, A. Milhem, and M. Abido, "Modelling of interior-mount LSPMSM under asymmetrical stator winding," *IET Electr. Power Appl.*, vol. 12, no. 5, pp. 693–700, May 2018, doi: 10.1049/iet-epa.2017.0525.

[8] D. S. B. Fonseca, C. M. C. Santos, and A. J. M. Cardoso, "Stator faults modeling and diagnostics of line-start permanent magnet synchronous motors," *IEEE Trans. Ind. Appl.*, vol. 56, no. 3, pp. 2590–2599, May 2020, doi: 10.1109/TIA.2020.2979674.

[9] L. S. Maraaba, Z. M. Al-Hamouz, and M. A. Abido, "Mathematical modeling, simulation and experimental testing of interior-mount LSPMSM under stator inter-turn fault," *IEEE Trans. Energy Convers.*, vol. 34, no. 3, pp. 1213–1222, Sep. 2019, doi: 10.1109/TEC.2018.2886137.

[10] L. S. Maraaba, S. Twaha, A. Memon, and Z. Al-Hamouz, "Recognition of stator winding inter-turn fault in interior-mount LSPMSM using acoustic signals," *Symmetry*, vol. 12, no. 8, p. 1370, Aug. 2020, doi: 10.3390/sym12081370.

[11] L. S. Maraaba, Z. M. Al-Hamouz, A. S. Milhem, and M. A. Abido, "Neural network-based diagnostic tool for detecting stator inter-turn faults in line start permanent magnet synchronous motors," *IEEE Access*, vol. 7, pp. 89014–89025, 2019, doi: 10.1109/ACCESS.2019.2923746.

[12] L. S. Maraaba, A. S. Milhem, I. A. Nemer, H. Al-Duwaish, and M. A. Abido, "Convolutional neural network-based inter-turn fault diagnosis in LSPMSMs," *IEEE Access*, vol. 8, pp. 81960–81970, 2020, doi: 10.1109/ACCESS.2020.2991137.

[13] A. Sapena-Bano, J. Burriel-Valencia, M. Pineda-Sanchez, R. Puche-Panadero, and M. Riera-Guasp, "The harmonic order tracking analysis method for the fault diagnosis in induction motors under time-varying conditions," *IEEE Trans. Energy Convers.*, vol. 32, no. 1, pp. 244–256, Mar. 2017, doi: 10.1109/TEC.2016.2626008.

[14] J. Alsalaet, S. Najim, and A. Ali, "Order tracking analysis using generalized Fourier transform with nonorthogonal basis," *J. Vib. Acoust.*, vol. 136, no. 6, pp. 1–35, Dec. 2014, doi: 10.1115/1.4028269.
[15] N. E. Huang, Z. Shen, S. R. Long, M. C. Wu, H. H. Shih, Q. Zheng, N.-C. Yen, C. C. Tung, and H. H. Liu, "The empirical mode decomposition and the Hilbert spectrum for nonlinear and non-stationary time series analysis," *Proc. Roy. Soc. London A, Math., Phys. Eng. Sci.*, vol. 454, no. 1971, pp. 903–995, Mar. 1998, doi: 10.1098/rspa.1998.0193.
[16] J.-C. Urresty, J.-R. Riba, and L. Romeral, "Diagnosis of interturn faults in PMSMs operating under nonstationary conditions by applying order tracking filtering," *IEEE Trans. Power Electron.*, vol. 28, no. 1, pp. 507–515, Jan. 2013, doi: 10.1109/TPEL.2012.2198077.
[17] M.-C. Pan, S.-W. Liao, and C.-C. Chiu, "Improvement on Gabor order tracking and objective comparison with Vold–Kalman filtering order tracking," *Mech. Syst. Signal Process.*, vol. 21, no. 2, pp. 653–667, Feb. 2007, doi: 10.1016/j.ymssp.2006.01.006.
[18] M. Riera-Guasp, M. Pineda-Sanchez, J. Perez-Cruz, R. Puche-Panadero, J. Roger-Folch, and J. A. Antonino-Daviu, "Diagnosis of induction motor faults via Gabor analysis of the current in transient regime," *IEEE Trans. Instrum. Meas.*, vol. 61, no. 6, pp. 1583–1596, Jun. 2012, doi: 10.1109/TIM.2012.2186650.
[19] S. Rajagopalan, J. A. Restrepo, J. M. Aller, T. G. Habetler, and R. G. Harley, "Nonstationary motor fault detection using recent quadratic time–frequency representations," *IEEE Trans. Ind. Appl.*, vol. 44, no. 3, pp. 735–744, May 2008, doi: 10.1109/TIA.2008.921431.
[20] J. Zarei, M. A. Tajeddini, and H. R. Karimi, "Fault diagnosis of induction motors broken rotor bars by pattern recognition based on noise cancelation," in *Proc. IEEE 23rd Int. Symp. Ind. Electron. (ISIE)*, Jun. 2014, pp. 2451–2456, doi: 10.1109/ISIE.2014.6865004.
[21] M. Pineda-Sanchez, M. Riera-Guasp, J. Roger-Folch, J. A. Antonino-Daviu, J. Perez-Cruz, and R. Puche-Panadero, "Diagnosis of induction motor faults in time-varying conditions using the polynomial-phase transform of the current," *IEEE Trans. Ind. Electron.*, vol. 58, no. 4, pp. 1428–1439, Apr. 2011, doi: 10.1109/TIE.2010.2050755.
[22] T. Ghanbari and H. Samet, "A Kalman filter based technique for stator turn-fault detection of the induction motors," *Int. J. Emerg. Electr. Power Syst.*, vol. 18, no. 6, p. 1, Dec. 2017, doi: 10.1515/ijeeps-2017-0071.
[23] A. Kiselev, A. Kuznietsov, and R. Leidhold, "Model based online detection of inter-turn short circuit faults in PMSM drives under non-stationary conditions," in *Proc. 11th IEEE Int. Conf. Compat., Power Electron. Power Eng. (CPE-POWERENG)*, Apr. 2017, pp. 370–374, doi: 10.1109/CPE.2017.7915199.
[24] J. Hang, S. Ding, J. Zhang, M. Cheng, W. Chen, and Q. Wang, "Detection of interturn short-circuit fault for PMSM with simple fault indicator," *IEEE Trans. Energy Convers.*, vol. 31, no. 4, pp. 1697–1699, Dec. 2016, doi: 10.1109/TEC.2016.2583780.
[25] J. R. Blough, D. L. Brown, and H. Vold, "The time variant discrete Fourier transform as an order tracking method," SAE Int., Cincinnati, OH, USA, Tech. Rep. 972006, May 1997, doi: 10.4271/972006.
[26] S. Gade, H. Herlufsen, H. Konstantin-Hansen, and N. J. Wismer, "Order tracking analysis," Brüel Kjær Tech. Rev., Denmark, Tech. Rep. 2, Aug. 1995.
[27] M. Akar, "Detection of a static eccentricity fault in a closed loop driven induction motor by using the angular domain order tracking analysis method," *Mech. Syst. Signal Process.*, vol. 34, nos. 1–2, pp. 173–182, Jan. 2013, doi: 10.1016/j.ymssp.2012.04.003.
[28] M. Zhu, B. Yang, W. Hu, G. Feng, and N. C. Kar, "Vold–Kalman filtering order tracking based rotor demagnetization detection in PMSM," *IEEE Trans. Ind. Appl.*, vol. 55, no. 6, pp. 5768–5778, Nov. 2019, doi: 10.1109/TIA.2019.2932692.
[29] M.-C. Pan and S.-W. Liao, "Biomedical signal reconstruction using Gabor spectral tracking technique," *Int. J. Inf. Acquisition*, vol. 3, no. 1, pp. 25–31, Mar. 2006, doi: 10.1142/s0219878906000794.
[30] M. F. Albright and S. Qian, "A comparison of the newly proposed Gabor order tracking technique vs. other order tracking methods," *SAE Trans.*, vol. 110, no. 6, pp. 1724–1738, 2001, doi: 10.4271/2001-01-1471.
[31] S. Qian, "Gabor expansion for order tracking," *Sound Vib.*, vol. 37, no. 6, pp. 18–22, 2003.
[32] Y. Lei, J. Lin, Z. He, and M. J. Zuo, "A review on empirical mode decomposition in fault diagnosis of rotating machinery," *Mech. Syst. Signal Process.*, vol. 35, nos. 1–2, pp. 108–126, Feb. 2013, doi: 10.1016/j.ymssp.2012.09.015.
[33] B.-G. Gu, "Study of IPMSM interturn faults Part I: Development and analysis of models with series and parallel winding connections," *IEEE Trans. Power Electron.*, vol. 31, no. 8, pp. 5931–5943, Aug. 2016, doi: 10.1109/TPEL.2015.2496142.
[34] H. Saavedra, J. C. Urresty, J. R. Riba, and L. Romeral, "Detection of interturn faults in PMSMs with different winding configurations," *Energy Convers. Manag.*, vol. 79, pp. 534–542, Mar. 2014, doi: 10.1016/j.enconman.2013.12.059.
[35] S. S. Moosavi, A. Djerdir, Y. Ait-Amirat, and D. A. Khaburi, "ANN based fault diagnosis of permanent magnet synchronous motor under stator winding shorted turn," *Electr. Power Syst. Res.*, vol. 125, pp. 67–82, Aug. 2015, doi: 10.1016/j.epsr.2015.03.024.
[36] J. Wexler and S. Raz, "Discrete Gabor expansions," *Signal Process.*, vol. 21, no. 3, pp. 207–220, Nov. 1990, doi: 10.1016/0165-1684(90)90087-F.
[37] Y. Guo and K. K. Tan, "Order-crossing removal in Gabor order tracking by independent component analysis," *J. Sound Vib.*, vol. 325, nos. 1–2, pp. 471–488, Aug. 2009, doi: 10.1016/j.jsv.2009.03.003.
[38] T. Wang, M. Zhang, Q. Yu, and H. Zhang, "Comparing the applications of EMD and EEMD on time–frequency analysis of seismic signal," *J. Appl. Geophys.*, vol. 83, pp. 29–34, Aug. 2012, doi: 10.1016/j.jappgeo.2012.05.002.
[39] X. Qin, Q. Li, X. Dong, and S. Lv, "The fault diagnosis of rolling bearing based on ensemble empirical mode decomposition and random forest," *Shock Vib.*, vol. 2017, pp. 1–9, Aug. 2017, doi: 10.1155/2017/2623081.
[40] Y. Amirat, M. E. H. Benbouzid, T. Wang, K. Bacha, and G. Feld, "EEMD-based notch filter for induction machine bearing faults detection," *Appl. Acoust.*, vol. 133, pp. 202–209, Apr. 2018, doi: 10.1016/j.apacoust.2017.12.030.
[41] J. Harmouche, C. Delpha, D. Diallo, and Y. Le Bihan, "Statistical approach for nondestructive incipient crack detection and characterization using Kullback–Leibler divergence," *IEEE Trans. Rel.*, vol. 65, no. 3, pp. 1360–1368, Sep. 2016, doi: 10.1109/TR.2016.2570549.
[42] Z. Mezni, C. Delpha, D. Diallo, and A. Braham, "Bearings ball fault detection using Kullback–Leibler divergence in the EMD framework," in *Proc. Prognostics Syst. Health Manage. Conf. (PHM-Chongqing)*, Oct. 2018, pp. 729–734, doi: 10.1109/PHM-Chongqing.2018.00130.
[43] J. Harmouche, C. Delpha, and D. Diallo, "Incipient fault detection and diagnosis based on Kullback–Leibler divergence using principal component analysis: Part II," *Signal Process.*, vol. 109, pp. 334–344, Apr. 2015, doi: 10.1016/j.sigpro.2014.06.023.
[44] L. Romeral, J. C. Urresty, J.-R. R. Ruiz, and A. G. Espinosa, "Modeling of surface-mounted permanent magnet synchronous motors with stator winding interturn faults," *IEEE Trans. Ind. Electron.*, vol. 58, no. 5, pp. 1576–1585, May 2011, doi: 10.1109/TIE.2010.2062480.
[45] Y. Wu, B. Jiang, and Y. Wang, "Incipient winding fault detection and diagnosis for squirrel-cage induction motors equipped on CRH trains," *ISA Trans.*, vol. 99, pp. 488–495, Apr. 2020, doi: 10.1016/j.isatra.2019.09.020.

ZAFER DOGAN (Member, IEEE) received the B.S. degree from the Technical Education Faculty and the M.S. and Ph.D. degrees from the Institute of Science, Marmara University. He is currently working with the Department of Electrical and Electronics Engineering, Faculty of Engineering and Architecture, Tokat Gaziosmanpasa University, as an Assistant Professor. His research interests include design of electrical machines, electrical energy systems diagnostics, and fault diagnosis in electrical machines.

KUBRA TETIK received the B.S. degree in electric and electronic engineering from Ondokuz Mayis University, Samsun, Turkey, in 2015, and the M.S. degree in electric and electronic engineering from Tokat Gaziosmanpasa University, Tokat, Turkey, in 2019.

Her research interest includes the detection of faults in electrical machines frequently used in industry using signal analysis.